Journal of Ultrafine Grained and Nanostructured Materials
https://jufgnsm.ut.ac.ir
Vol. 52, No.1, June 2019, pp. 122-132
Print ISSN: 2423-6845 Online ISSN: 2423-6837
DOI: 10.22059/JUFGNSM.2019.01.13

Immobilization of cobalt doped rutile TiO_2 on carbon nanotubes walls for efficient photodegradation of 2,4-dichlorophenol under visible light

Pejman Monazzam[1],Azadeh Ebrahimian Pirbazari*[,2],Behnam Fakhari Kisomi[3],Ziba Khodaee[4]

[1]Faculty of Caspian, College of Engineering, University of Tehran, Rezvanshahr, Iran.

[2]Hybridnanomaterials and Environment Laboratory, Faculty of Fouman, College of Engineering, University of Tehran, Iran.

[3]Faculty of Chemical Engineering, College of Engineering, University of Tehran, Iran.

[4]University of Applied Science and Technology, Guilan, Iran.

Recieved: 15 March 2019; Accepted: 18 May 2019

** Corresponding author email: aebrahimian@ut.ac.ir*

ABSTRACT

In this work, we focused on improvement of rutile-type TiO_2 degradation efficiency by cobalt doping and decorating on carbon nanotubes walls (CNTs) (Co-TiO_2/CNTs). We also synthesized pure TiO_2, Co-TiO2 and TiO2/CNTs samples for control expriments.The textural and morphology features of the samples were characterized by a range of analyses including: XRD, FESEM/EDX. FTIR, TEM, UV-Vis DRS and N_2 physisorption. The XRD results indicated that we obtained rutile phase as the major phase for TiO_2 with crystal size between 18-22 nm. The band gap energy of the samples were calculated from DRS analysis and Kubelka-Munk spectra and obtained 2.88, 2.38,2.97 and 2.20 eV for TiO2, Co-TiO2, TiO2/CNTs and Co-TiO2/CNTs respectively. The effectiveness of the samples was examined through degradation of 2,4-dichlorophenol (2,4-DCP) as a model of organic pollutants in the synthetic wastewater under visible light. We achieved 27% and 50% visible light degradation of 2,4-DCP in the presence of pure TiO_2 and Co-TiO_2/CNTs after 180 min irradiation, respectively. The high visible light activity of Co-TiO_2/CNTs sample could be approved that the presence of cobalt and CNTs reduced the band gap energy and sensitize TiO_2 surface to visible light. The mechanism for degradation of 2,4-DCP by Co-TiO_2/CNTs photocatalyst under visible light was proposed.

Keywords: *Cobalt; CNTs; Rutile; TiO_2; Visible light degradation; 2,4-dichlorophenol.*

1. Introduction

The expansion of degradation efficiency of TiO_2 in the visible light region is essential for decontamination of water pollutants. Many researchers made the efforts on the alteration of TiO_2 for improving of its efficiency under visible light by doping of noble, transition and rare earth metals [1, 2] and immobilization on different supports including zeolite, alumina, activated carbon and carbon nanotubes (CNTs)[3-5]. Another objective of surface modification of TiO_2 is to restrain the electrons and holes recombination by encouraging the charge isolation to improve the degradation performance [6, 7]. Cobalt as one of the most valuable dopants among the transition metals can develop the light response and degradation activity

of TiO_2. Recently, Ebrahimian et al. [8] prepared cobalt doped TiO_2 nanoparticles by hydrothermal method and the synthesized samples showed a great absorption range in the visible region. Iwasaki et al. [9] reported that doping of Co^{2+} into TiO_2 lattice could extend the absorption edge of TiO_2 and improve degradation performance of it under UV irradiation and visible light. The degradation performance of TiO_2 can be improved under UV by using CNTs in TiO_2 composite and surface features are changed to attain sensitivity to visible light [10]. Moreover, using CNTs in the structure of TiO_2 composite changes morphology and the particle dimension of TiO_2 [11]. Furthermore, the photocatalytic activity is greatly affected by CNTs as dispersing agent, adsorbent and photosensitizer [12].

The one dimensional nature of CNTs provides easy movement of charge carriers through nanotubes with no scattering causing ballistic transport that minimizes Joule heating and consequently, currents with very large densities transfer easily[13]. These transporting features of CNTs causes a suitable means of directing the flow of photoinduced electrons and holes and increase the life of them [14].

In our previous study[15], we investigated the effect of cobalt doping on the phase formation of TiO_2 and achieved anatase as the major phase for the prepared nanocomposites. In the current study, we focused on the synthesis of cobalt doped TiO_2 with rutile major phase and decorated on the walls of CNTs. The textural and morphology features of the obtained photocatalysts were characterized by XRD, FTIR, DRS, FESEM/EDX, TEM and N_2physisorption analyses. The effectiveness of the obtained samples was assessed through degradation of synthetic wastewater containing 2,4-dichlorophenol (2,4-DCP) under visible light.

2. Materials and Methods

2.1. Materials and reagents

Cobalt (II) chloride hexahydrate ($CoCl_2.6H_2O$) (Merck, No.102539),Titanium isopropoxide (TIP) (Merck No. 8.21895), ethanol (Merck No. 818760), high-purity 2,4-DCP, 98%, (Merck No. 803774), and carboxylic groups-functionalized CNTs with diameter of the 10-20 nm and the length of 0.5-2.0 μm provided by Neutrino Corporation (Iran) were used in this study. Deionized water was used in all experiments.

2.2. Preparation of Co-TiO_2/CNTs nanocomposite

Co-TiO_2/CNTs photocatalyst was synthesized through a sol-gel technique. 0.96 g of $CoCl_2.6H_2O$, 20 mL TIP and 60 mL ethanol were agitated for 2h (Solution A). Next, solution B, 40 mL ethanol, 10 mL deionized water, 4 mL hydrochloric acid and 0.08 g CNTs were poured into the solution A and agitated for 12h at ambient temperature. The sol was generated after stirring for 12h and aging at ambient temperature for 24h. Then it was evaporated at 80 °C for 8h to obtain the dried powder. Lastly, the Co-TiO_2/CNTs sample was obtained by calcinating the resulted powder at 450 °C under air for 2h. Pure TiO_2, Co-TiO_2 and TiO_2/CNTs samples were prepared through the similar method (Table 1). We selected the amount of $CoCl_2.6H_2O$ and CNTs to obtain 6 and 8% weight percentage of cobalt and CNTs respectively for binary Co-TiO_2 and TiO_2/CNTs nanocomposite.

2.3. Characterization

The XRD analysis was performed using a Siemens D5000 instrument (Germany) while Cu K_α radiation was employed as the X-ray source. The diffractograms were recorded in the 2θ= 20 -80°. Morphology of the samples was identified by scanning electron microscopy (SEM) (Vegall-Tescan Company), which was coupled with an energy dispersive X-ray (EDX) detector. The diffuse reflectance UV–Vis spectra (DRS) of the samples were recorded by an Ava Spec-2048TEC spectrometer.Physisorption of nitrogen was studied by a Quantachrome Autosorb-1-MP (Micromeritics) in order to measure BET areas through static nitrogen physisorption. The samples were degassed at 200 °C for 2 h prior to the sorption measurement. FTIR analysis was applied

Table 1- Nomenclature of the prepared samples

Samples	TIP (ml)	HCl (ml)	$CoCl_2.6H_2O$ (g)	Ethanol (ml)	H_2O (ml)	CNTs (g)
TiO_2	20	4	-	100	10	-
Co-TiO_2	20	4	0.96	100	10	-
TiO_2/CNTs	20	4	-	100	10	0.08
Co-TiO_2/CNTs	20	4	0.96	100	10	0.08

to determine the surface functional groups, using FTIR spectroscope (FTIR-2000, Bruker, USA), where the spectra were recorded from 4,000 to 400 cm^{-1}.

2.4. Photodegradation of 2,4-DCP

We selected 2,4-DCP as a model of organic pollutants to examine degradation performance of the obtained samples. We used Halogen, ECO OSRAM 500W lamp (350 to 800 nm, with the most intense peak at 575 nm) as visible light source. In each degradation experiment, the beaker containing optimum amount of photocatalyst and 100 mL 2,4-DCP aqueous solution (40 mg/L) was agitated first for 10 min, in the dark, for adsorption/desorption equilibrium and after this time, the lamp turned on for 180 min. At certain times, 2 mL of the solution was taken and filtered to eliminate the photocatalyst and analyzed using Rayleigh UV-2601 UV/VIS spectrophotometer (λ_{max}= 227nm).

3. Results&Discussion

3.1. X-ray diffraction analysis

The XRD patterns of the synthesized samples have been presented in Fig. 1. In XRD pattern of pure TiO_2 (Fig. 1a), the diffractions at 2θ= 27.48°, 36.14°, 41.24° and 54.34° with Miller indexes (110), (101), (111) and (211), respectively are the main diffractions of polycrystalline with a rutile structure[16]. The diffractions at 2θ= 37.80°, 48.18°, and 54.09° are the key peaks for the anatase crystalline phase of TiO_2 (JCPDS 21-1272). The XRD pattern showed the synthesized TiO_2 comprising predominant rutile crystalline phase and a small amount of anatase crystalline phase. Moreover, the XRD pattern of Co-TiO_2 sample (Fig. 1b) did not indicate any cobalt phase, so it can be concluded that cobalt ions homogenously dispersed into the TiO_2 crystallites and represented rutile phase as major phase for TiO_2 [17, 18].

In XRD pattern of TiO_2/CNTs (Fig. 1c), the main diffraction of CNTs at 2θ=25.5°[19] has not been detected and it may be overlapped with the main diffraction of anatase TiO_2 at 2θ=25.3°. Furthermore, it may be attributed to the significant difference between the mass percent of CNTs and TiO_2 and the low crystallinity of CNTs [13]. In the XRD pattern of Co-TiO_2/CNTs (Fig. 1d), the main diffractions of rutile crystalline phase were detected for TiO_2.

The mean TiO_2 crystal size for each samples was calculated at 2θ= 27.48° by using Scherrer's equation (Eq. (1))[20]:

$$D= K\lambda/\beta \cos\theta \qquad \text{(eq. 1)}$$

Where D represents the mean crystallite size of TiO_2 in nm, λ is the wavelength of X-ray (1.54056 Å), β refers to the diffraction full width at half maximum (FWHM) in radian, K represents a coefficient (0.89) and θ is the diffraction angle at 2θ= 27.48°. The TiO_2 crystal size for all the obtained samples is in the nanosized range (Table 2).The mean crystallite size of TiO_2 in Co-TiO_2 and Co-TiO_2/CNTs samples is smaller compared with pure TiO_2, it can be stated that adding cobalt to titania delays the growth of TiO_2 nanoparticles. It seems that cobalt ions form complex with the TiO_2

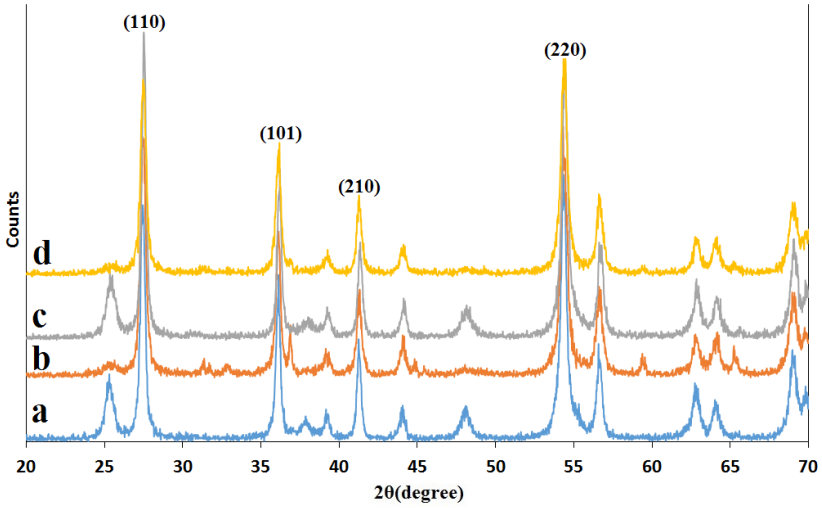

Fig. 1- The XRD patterns of a) TiO_2, b) Co-TiO_2, c) TiO_2/CNTs and d) Co-TiO_2/CNTs.

surface oxygen, hence, suppress the growth of TiO_2 crystallite[21].

The lattice parameters (a=b≠c) of tetragonal crystalline structure were obtained for (110) crystal plane of rutile phase using Eq. (2):

$$1/d^2= (h^2 +k^2)/a^2 + l^2/c^2 \quad \text{(eq. 2)}$$

Considering the interplanar spacing (d_{hkl}), the distance between adjacent planes in the set (hkl) can be determined using the Bragg law (Eq. (3)):

$$d_{hkl}= \lambda/2 \sin\theta \quad \text{(eq. 3)}$$

The volume of cell (tetragonal one) was computed by Eq. (4):

$$V= a^2c \quad \text{(eq. 4)}$$

Where a and c are considered lattice factors. Table 2 displays the lattice factors of the synthesized samples. The achieved values for the lattice factors of TiO_2 in the synthesized samples matched well with the TiO_2 rutile structure [16]. The calculated values for the lattice factors of pure TiO_2 are in well matched with the rutile phase of TiO_2 [16]. No other impurity peaks are detected, which ensure high purity of TiO_2 powder used for Co doping. The diffraction patterns of the synthesized samples do not show any extra peaks confirming that the rutile phase is not troubled upon Co doping in TiO_2. A significant difference between ionic radii of the dopant and the host ions (i.e., Co^{2+}: 0.745 Å and Ti^{4+}: 0.605 Å, with a coordination number of 6) is predictable to cause a small enhancement of the TiO_2 unit cell size.

3.2. Diffuse reflectance spectroscopy analysis

The solid-state UV-Visible spectra (Fig. 2A) were recorded for all the samples. In the DR spectrum of pure TiO_2, absorption peak around 400 nm can be attributed to the charge-transfer from the valence band of the oxide anions to the conduction band of the Ti^{4+}cations [21].

The diffuse reflectance spectra of the Co-TiO_2 and Co-TiO_2/CNTs samples (Figs. 2b, d), consist of additional broad absorption peak between 500 to 750 nm. The genesis of absorption peak is attributed to Co^{2+}/Ti^{4+}charge-transfer interaction [22]. This may also be a reason for high degradation efficiency of these samples in the visible region compared with pure TiO_2. We also measured the energy of band gap of the synthesized samples using the diffuse reflectance spectra according to

Table 2- Phase, crystal size and lattice parameters of the prepared samples

Sample	Major Phase	Crystal size (nm)	a=b (Å)	c (Å)	Cell volume ($Å^3$)
TiO_2	Rutile	21.540	4.598	2.957	62.505
Co-TiO_2	Rutile	20.466	4.600	2.956	62.561
TiO_2/CNTs	Rutile	21.261	4.588	2.951	62.110
Co-TiO_2/CNTs	Rutile	18.190	4.593	2.951	62.266

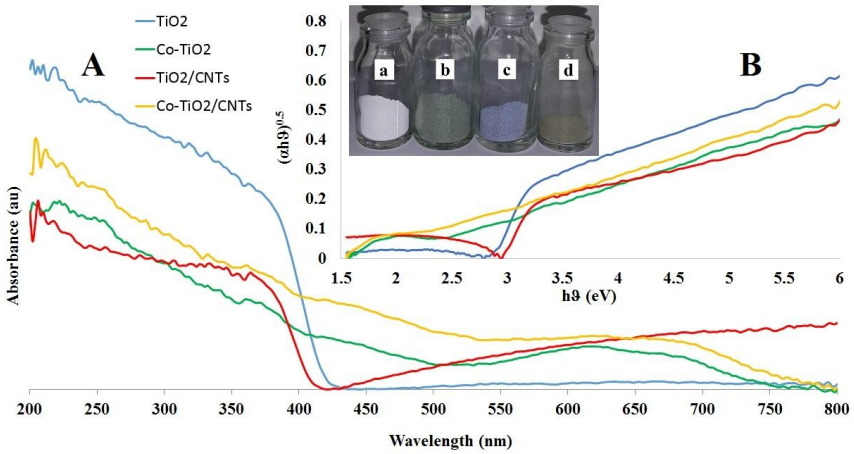

Fig. 2- Diffuse reflectance spectra and B: Kubelka-Munk plots for the band gap energy calculation of a)TiO_2 b)Co-TiO_2 c) TiO_2/CNTs and d) Co-TiO_2/CNTs.

Eq. (5)[23].

$$[F(R)\ h\upsilon]^{0.5} = A\ (h\upsilon - E_{bg}) \qquad \text{(eq. 5)}$$

Where A is constant, F(R)is the function of Kubelka-Munk (Fig. 2B), and E_{bg} is the band gap. The E_{bg} data of samples have been presented in Table 3. The pure TiO_2 showed high reflection within the visible light region (>400 nm), while the samples comprising cobalt showed lower reflection in the visible region, meaning that visible light photoresponse of the cobalt doped samples was increased. Red shifts found for the cobalt doped TiO_2 samples showed that the band gap energy of the samples was decreased gradually (Table 3). The band gap of samples containing cobalt decreased compared with TiO_2. It can be clearly seen that doping cobalt in the TiO_2 structure affects the optical features of TiO_2 significantly. It is evident that, the degradation activity of the Co-TiO_2 and Co-TiO_2/CNTs is greatly shifted into the visible light region, and exhibits a band gap narrowing 2.375 and 2.200 eV compared with that of pure TiO_2 (2.880 eV).It is explained in literatures that the presence of transition metals might introduce new intra band gap states, giving the TiO_2 the capacity to absorb light at lower energy levels, thus, promoting the absorption on the visible part of the spectrum. The incorporation of the transition metal provides d orbitals just below the conduction band. These d orbitals are then able to receive electrons from the valence band, thus lowering the band gap energy [24].

3.3. FESEM/EDX and TEM analyses

Fig. 3 displays the FESEM images of the synthesized samples. FESEM images show that all the samples are slightly agglomerated and in the case of TiO_2/CNTs and Co-TiO_2/CNTs samples (Figs. 3c, d), TiO_2 and Co-TiO_2 nanoparticles are

Table 3- Color and band gap energy of the prepared samples

Samples	E_{bg}(eV)	Color
TiO_2	2.880	White
Co-TiO_2	2.375	Green
TiO_2/CNTs	2.970	Gray
Co-TiO_2/CNTs	2.200	Slime Green

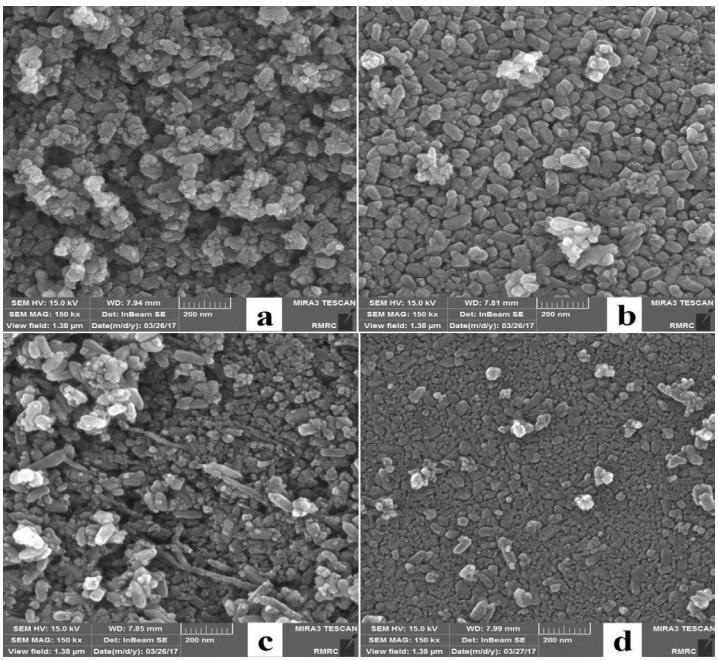

Fig. 3- FESEM images of a) TiO_2, b) Co-TiO_2, c) TiO_2/CNTs and d) Co-TiO_2/CNTs.

decorated on the CNTs walls. The FESEM analysis and XRD calculations (Table 2) display that the existence of cobalt and CNTs has prevented increasing the dimension of TiO_2 particles (Table 2).

The EDX results were utilized to study the elemental composition of the samples (Fig. 4). The elemental analysis confirms the existence of C, Ti, O and Co elements in these samples. The EDX patterns of the samples (Fig. 4) display two peaks about 0.2 and 4.5 keV. The strong peak is related to the bulk TiO_2 and the less strong one is related to the surface TiO_2. Fig. 4 shows the peaks of cobalt at 0.6, 6.9 and 7.5 keV. The less strong peak is allocated to cobalt in the TiO_2 lattices [21, 25]. Fig. 5 demonstrates elemental mapping images of the synthesized samples. According to the elemental mapping mode, cobalt was greatly and homogeneously dispersed in the TiO_2 lattice. This implies good interaction of cobalt and TiO_2 over the sol-gel synthesis procedure. The elemental analysis of the samples showed the existence of cobalt atoms and CNTs in the powder structure, as the opposite of XRD patterns.

Fig. 6 shows the TEM image of Co-TiO_2/CNTs nanocomposite. According to these images, Co-TiO_2 NPs are dispersed on the wall of CNTs.

3.4. N_2 physisorption analysis

The results of N_2 adsorption/desorption isotherms are shown in Fig.7. The sorption isotherms for the prepared samples correspond to the type IV isotherm based on the classification of IUPAC [26]. Textural and structural parameters of the obtained samples have been presented in Table 4. The specific surface areas calculated according to BET and the average pore diameter and pore volumes were extracted from the desorption branch based on the BJH model. Cobalt addition resulted in a reduction in both surface area and pore volume for the Co-TiO_2 and Co-TiO_2/CNTs samples. These variations could be attributed to the developed sintering and/or agglomeration of TiO_2 or to the formation of $CoTiO_3$ compound [22].

Table 4- Textural and structural parameters of the prepared samples

Sample	S_{BET} (m^2/g)	Average pore diameter (nm)	Pore volume (cm^3/g)
TiO_2	41.21	19.02	0.20
Co-TiO_2	34.28	25.75	0.13
TiO_2/CNTs	46.84	21.10	0.25
Co-TiO_2/CNTs	33.70	17.27	0.15

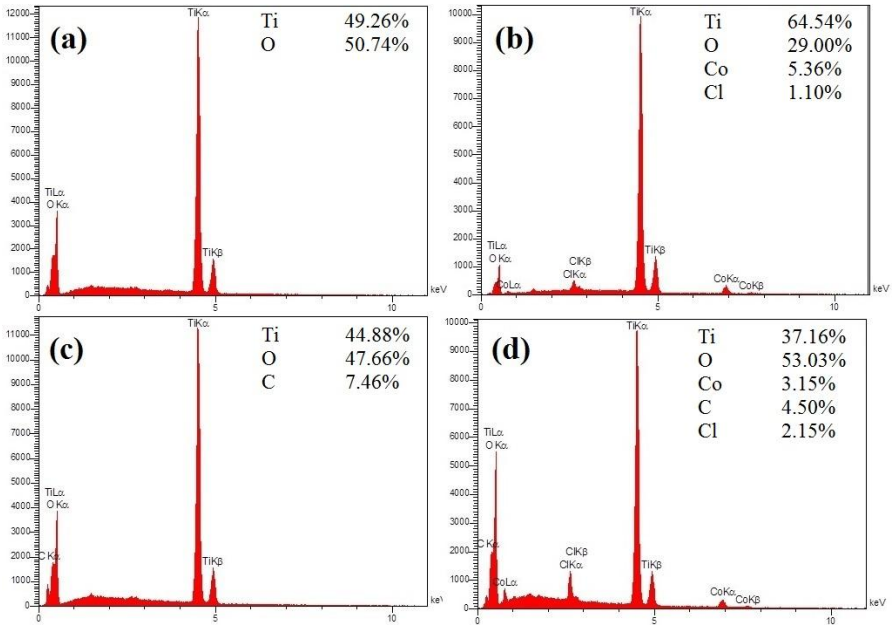

Fig. 4- EDX spectra and elemental chemical analysis (wt%) of a) TiO_2, b) Co-TiO_2, c) TiO_2/CNTs and d) Co-TiO_2/CNTs.

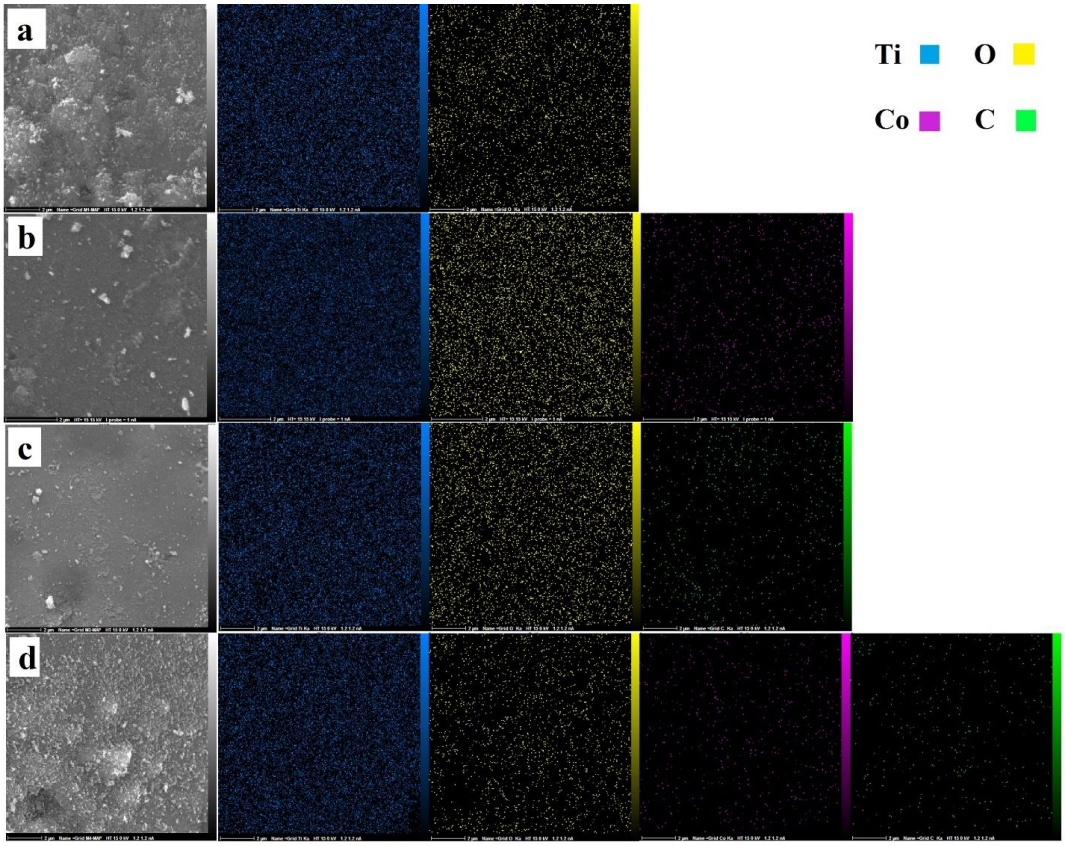

Fig. 5-Elemental mapping of a)TiO_2, b)Co-TiO_2, c) TiO_2/CNTs and d) Co-TiO_2/CNTs.

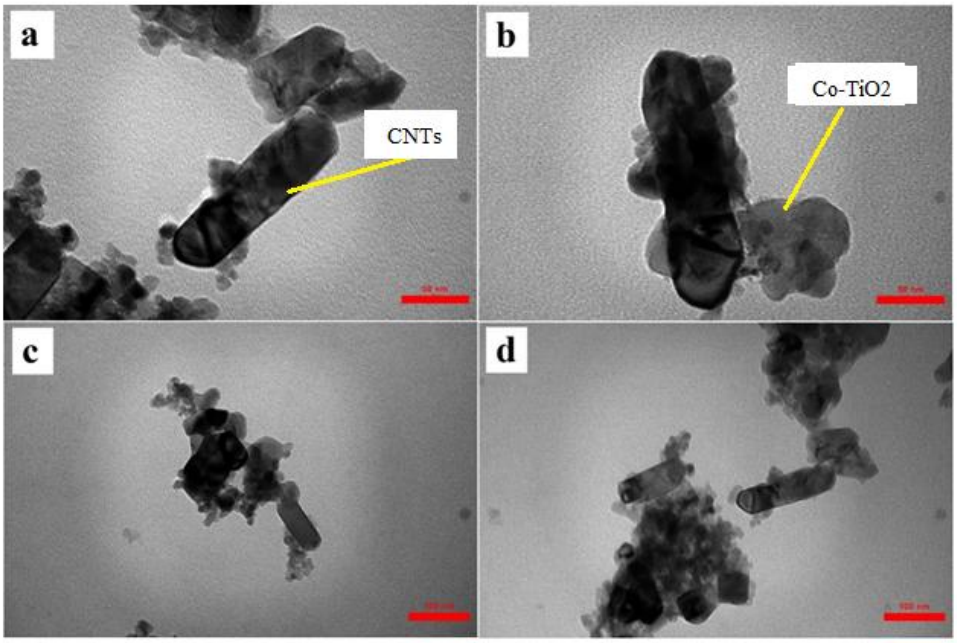

Fig. 6-TEM images of Co-TiO_2/CNTs nanocomposite at a, b) 50 nm and c, d) 100 nm.

3.5. FTIR spectroscopy analysis

Fig. 8 shows the FTIR spectra of the synthesized samples. The peak positioned at 3,350–3,450 cm^{-1} is assigned to O–H stretching vibration for all the samples. The peaks appearing at 1,620–1,635 cm^{-1} were attributed to H–O–H bending vibration mode of physically adsorbed water [27]. The strong vibration in the range of 700-500 cm^{-1} is attributed to stretching vibrations of Ti–O–Ti bond [28]. The weak peak at about 514 cm^{-1} assigned to stretching vibrations of Co–O emerged a little [29], the Co–O vibration is not strong because of the broad spectrum of TiO_2 and a small amount of Co dopant. FT-IR results reminded the formation of a small part of Co–O bond. It was probably the existence of Co–O bond that hindered the recombination of

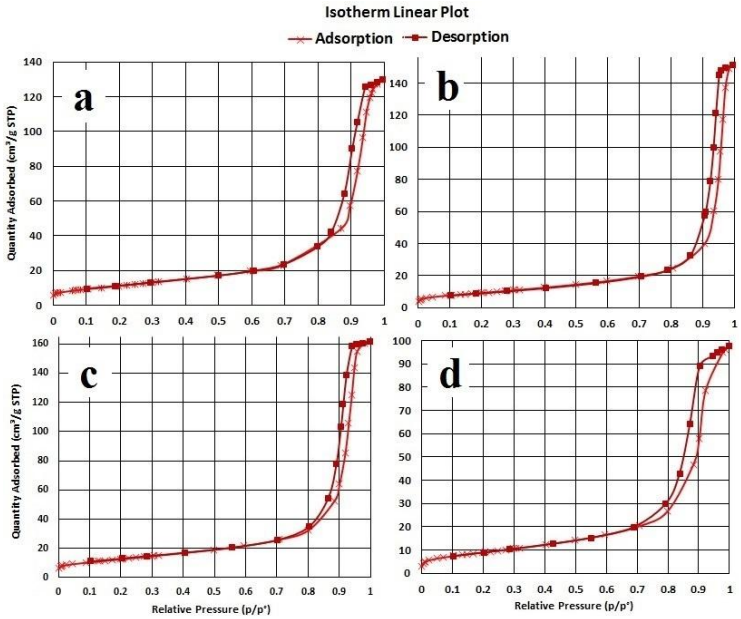

Fig. 7- N_2 adsorption–desorption isotherms for a)TiO_2, b)Co-TiO_2, c) TiO_2/CNTs and d) Co-TiO_2/CNTs.

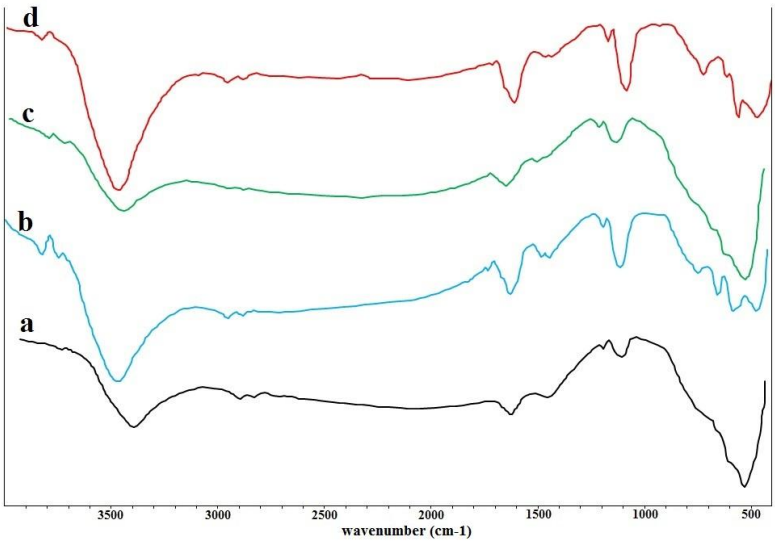

Fig. 8- The FTIR spectra of a)TiO_2, b)Co-TiO_2, c) TiO_2/CNTs and d) Co-TiO_2/CNTs.

generated photo holes and photoelectrons [30].

3.6. Degradation of 2,4-DCP

The degradation activity of 2,4-DCP with the synthesized samples under visible light presented in Fig. 9. Amongst the prepared samples, the photocatalytic activity of the Co-TiO_2/CNTs was the maximum and 50% degradation of 2,4-DCP achieved following 180 min irradiation under visible light. In the same conditions, we obtained 27%, 32% and 35% degradation of 2,4-DCP in the presence of pure TiO_2, Co-TiO_2 and TiO_2/CNTs samples respectively.

The two basic factors that are responsible for the activity of photocatalysts include surface area and light absorption capacity [21]. The DRS analysis results (Fig. 2) show that light absorption capacity of the prepared samples are different and increase with addition of cobalt in visible region. Therefore, addition of cobalt has two opposite effects on the degradation activity of the samples; increasing light absorption capacity and decreasing surface area. The degradation activity depends on which one of these is the dominant factor [8].

The higher degradation activity of Co-TiO_2/CNTs can be noticed that the presence of CNTs and cobalt clearly led to a synergetic impact on 2,4-DCP degradation and cause a larger photocatalytic performance. The more degradation activity of Co-TiO_2/CNTs nanocomposite may be described as firstly, the Co doped into TiO_2 could efficiently capture the photo-induced electrons and holes, which controlled combining photoinduced charge carriers and increased the degradation performance. Secondly, there are more surface hydroxyl groups in Co-TiO_2/CNTs samples compared with the pure TiO_2 which would be helpful for 2,4-DCP adsorption . The creation of hydroxyl radicals could be facilitated by the abundant hydroxyl groups adsorbed on the catalyst surface that could optimize the degradation procedure of the 2,4-DCP adsorbed on the surface[5]. Moreover, there is a synergetic impact among CNTs and TiO_2, and CNTs playing role as a photosensitizer. The photo-induced electrons can be trapped by CNTs and so, superoxide radical ion and/or hydroxyl radical is formed on the TiO_2 surface that they play role in degrading the organic compound. It can be suggested that charge on the surface of TiO_2 in the combined catalysts is increased due to the presence of CNTs. The surface charge may cause alterations of the fundamental procedure of electron/hole pair creation while using visible light [13]. Therefore, it may be the single interaction between TiO_2 and CNTs that endows the ternary nanocomposite with a higher catalytic activity in the degradation of 2,4-DCP than pure TiO_2. In the case of samples comprising cobalt, the Co^{2+} trapped electrons which then moved to he absorbed O_2 for reaching a greater photocatalytic activity. According to the literature

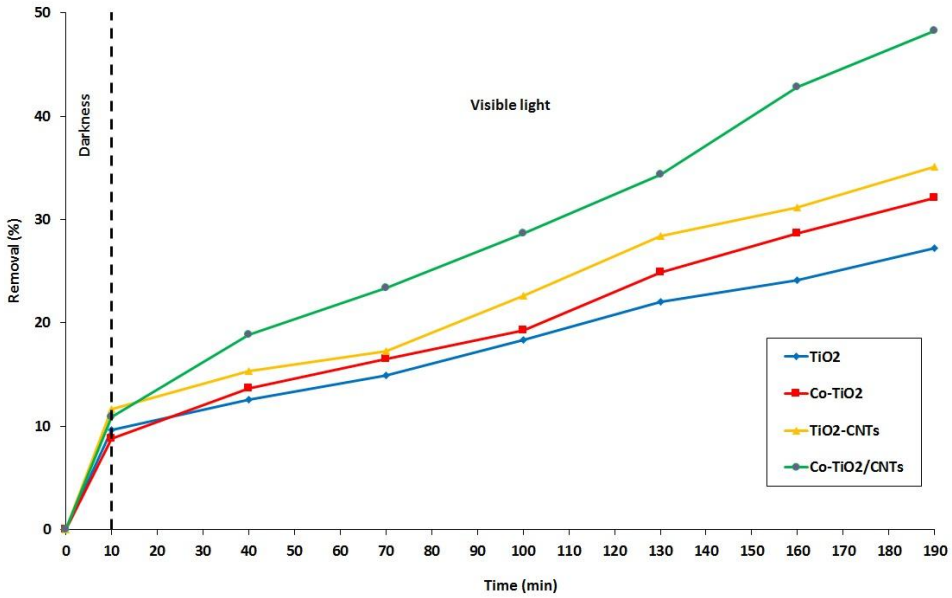

Fig. 9- Photodegradation of 2,4-DCP in the presence of the prepared samples under visible light. (Initial concentration of 2,4-DCP, 40 mg /L; volume, 100 mL;catalyst dosage, 10 mg and Irradiation time: 180 min)..

[31], with the replacement for Ti^{4+} by Co^{2+}in TiO_2 crystal structure, the catalyst can introduce a new levels of impurity to the conduction band of TiO_2 and the electrons can be moved from the valence band to these impurity levels, causing a narrowing of the band gap. This fact shows the presence of higher number of photogenerated electrons and holes which can be introduced for participating in the photocatalytic reactions [32]. Though, recombining photogenerated electrons and holes is one of the most important parameters that decline the photoactivity of the TiO_2 catalyst. Any parameter, which suppresses the recombination of electron-hole, will increase the photocatalytic performance [33]. Generally, if the dimension of doping metal ion is very similar to Ti^{4+}, entering metal ion into the TiO_2 crystal interstitial site is very probable. The doping metal ion placed mostly on the shallow surface of TiO_2 can induce defects. These defects can become the centers of shallow electrons or holes traps, which would powerfully progress separation process of an electron-hole pair. Therefore, the photocatalyst will have a great photocatalytic performance [34]. Our suggested mechanism for photodegradation of 2,4-DCP by Co-TiO_2/CNTs photocatalyst is shown in Fig.10.

4. Conclusions

In summary, the photocatalytic efficiency of rutile-type TiO_2 was successfully improved by cobalt doping and decorating on CNTs walls. It was found that the Co-TiO_2/CNTs sample presented enhanced degradation of 2,4-dichlorophenol (2,4-DCP) and exhibited expansion in spectral response range shifted to the visible region. We obtained 27% and 50% visible light degradation of 2,4-DCP in the presence of TiO_2 and Co-TiO_2/CNTs respectively after 180min irradiation. The presence of CNTs and cobalt dopant in Co-TiO_2/CNTs nanocomposite promoted the separation of photoinduced charge carriers and extended the absorption spectrum of TiO_2 into visible region.

Acknowledgements

The authors wish to acknowledge the financial support of University of Tehran for supporting of this research. Also, the author wish to acknowledge the financial support of Iran Nanotechnology

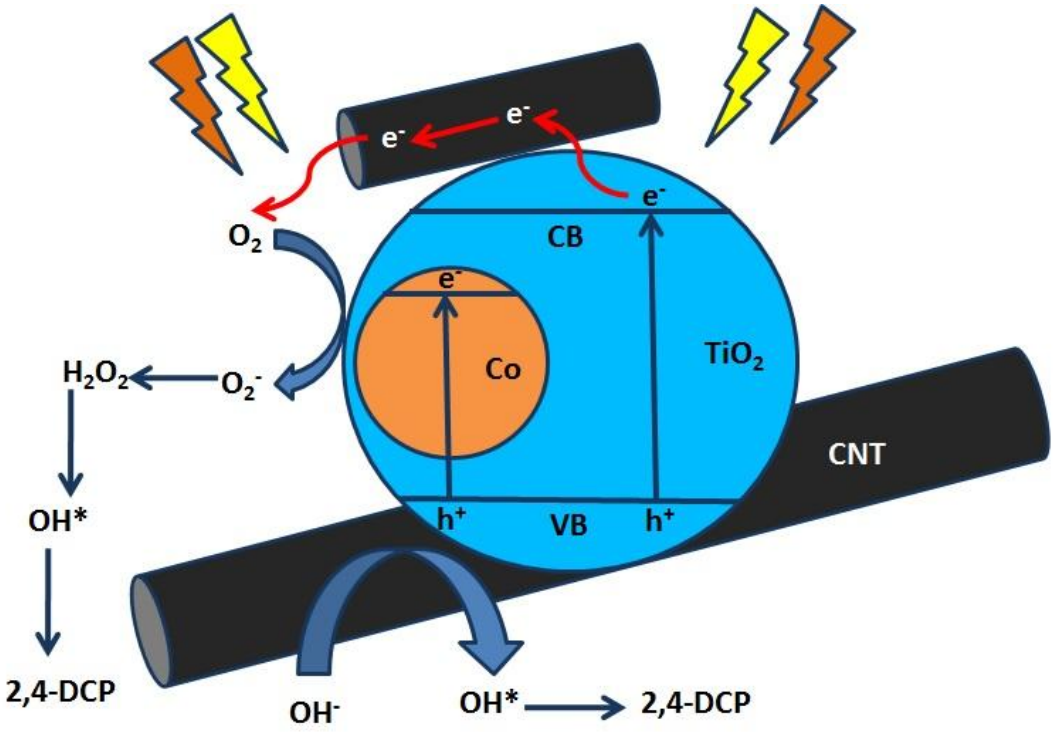

Fig. 10-Suggested mechanism for 2,4-DCP degradation in the presence of Co-TiO_2/CNTs under visible light.

Initiative Council (INIC) Foundation (Grant No: 122611).

References

1. Sarteep Z, Pirbazari AE, Aroon MA, Silver Doped TiO_2 Nanoparticles: Preparation, Characterization and Efficient Degradation of 2,4-dichlorophenol Under Visible Light. Journal of Water and Environmental Nanotechnology. 2016;1;135-144.
2. Wang S, Zhou S, Photodegradation of methyl orange by photocatalyst of CNTs/P-TiO_2 under UV and visible-light irradiation. Journal of hazardous materials. 2011;185;77-85.
3. Saleh TA, Gondal M, Drmosh Q, Yamani Z, Al-Yamani A, Enhancement in photocatalytic activity for acetaldehyde removal by embedding ZnO nano particles on multiwall carbon nanotubes. Chemical Engineering Journal. 2011;166;407-412.
4. Zhang J, Huang Zh, Yong X, Kang Fy, Carbon-coated TiO_2 composites for the photocatalytic degradation of low concentration benzene. New Carbon Materials. 2011;26;63-70. 26 (2011).
5. Yang Q, Deng Y, Hu W, Preparation of alumina/carbon nanotubes composites by chemical precipitation. Ceramics International. 2009;35;1305-1310.
6. Feng H, Zhang MH, Liya EY, Hydrothermal synthesis and photocatalytic performance of metal-ions doped TiO_2. Applied Catalysis A: General. 2012;413;238-244.
7. Pasikhani JV, Gilani N, Pirbazari AE, Improvement the wastewater purification by TiO_2 nanotube arrays: The effect of etching-step on the photo-generated charge carriers and photocatalytic activity of anodic TiO_2 nanotubes. Solid State Sciences. 2018;84;57-74.
8. Pirbazari AE, Monazzam P, Kisomi BF, Co/TiO_2 nanoparticles: preparation, characterization and its application for photocatalytic degradation of methylene blue. Desalination and Water Treatment. 2017;63;283-292.
9. Iwasaki M, Hara M, Kawada H, Tada H, Ito S, Cobalt Ion-Doped TiO_2 Photocatalyst Response to Visible Light. Journal ofColloid and Interface Science. 2000;224;202-204.
10. Wang H, Wang HL, Jiang WF, Li ZQ, Photocatalytic degradation of 2, 4-dinitrophenol (DNP) by multi-walled carbon nanotubes (MWCNTs)/TiO_2 composite in aqueous solution under solar irradiation. Water research. 2009;43;204-210.
11. Huang B, Yang Y, Chen X, Ye D, Preparation and characterization of CdS–TiO2 nanoparticles supported on multi-walled carbon nanotubes. Catalysis Communications. 2010;11;844-847.
12. Peining Z, Nair AS, Shengyuan Y, Ramakrishna S, TiO_2–MWCNT rice grain-shaped nanocomposites—Synthesis, characterization and photocatalysis. Materials Research Bulletin. 2011;46;588-595.
13. Wei B, Vajtai R, Ajayan P, Reliability and current carrying capacity of carbon nanotubes. Applied Physics Letters. 2001;79;1172-1174.
14. Xia XH, Jia ZJ, Yu Y, Liang Y, Wang Z, Ma LL, Preparation of multi-walled carbon nanotube supported TiO_2 and its photocatalytic activity in the reduction of CO_2 with H_2O. carbon. 2007;45;717-721.
15. Laghani SN, Pirbazari AE, Photocatalytic Treatment of Synthetic Wastewater Containing 2,4 dichlorophenol by Ternary MWCNTs /Co-TiO_2 Nanocomposite Under Visible Light. Journal of Water and Environmental Nanotechnology. 2017;2;290-301.
16. Ogata M, Kadowaki K, Ijiri M, Takemoto Y, Terashima K, Wakita T, Yokoya T, Muraoka Y, Effect of aliovalent dopants on the kinetics of spinodal decomposition in rutile-type TiO_2-VO_2. Journal of the European Ceramic Society. 2017;37;3177-3183.
17. Jiang P, Xiang W, Kuang J, Liu W, Cao W, Effect of cobalt doping on the electronic, optical and photocatalytic properties of TiO_2. Solid State Sciences. 2015;46;27-32.
18. Preethi T, Abarna B, Vidhya K, Rajarajeswari G, Sol–gel derived cobalt doped nano-titania photocatalytic system for solar light induced degradation of crystal violet. Ceramics International. 2014;40;13159-13167.
19. Ahmmad B, Kusumoto Y, Somekawa S, Ikeda M, Carbon nanotubes synergistically enhance photocatalytic activity of TiO_2. Catalysis Communications. 2008;9;1410-1413.
20. Khan M, Cao W, Cationic (V, Y)-codoped TiO_2 with enhanced visible light induced photocatalytic activity: A combined experimental and theoretical study. Journal of Applied Physics. 2013;114;183514.
21. Hamadanian M, Reisi-Vanani A, Majedi A, Sol-gel preparation and characterization of Co/TiO_2 nanoparticles: application to the degradation of methyl orange. Journal of the Iranian Chemical Society. 2010;7;52-58.
22. Ganesh I, Gupta A, Kumar P, Sekhar PC, Radha K, Padmanabham G, Sundararajan G, Preparation and characterization of Co-doped TiO_2 materials for solar light induced current and photocatalytic applications. Materials Chemistry and Physics. 2012;135;220-234.
23. Kumar S, Khanchandani S, Thirumal M, A.K. Ganguli AK, Achieving enhanced visible-light-driven photocatalysis using type-II $NaNbO_3$/CdS core/shell heterostructures. ACS applied materials & interfaces. 2014;6;13221-13233.
24. Zhu J, Chen F, Zhang J, Chen H, Anpo M, Fe^{3+}-TiO_2 photocatalysts prepared by combining sol–gel method with hydrothermal treatment and their characterization. Journal of Photochemistry and Photobiology A: Chemistry. 2006;180;196-204.
25. Venkatachalam N, Palanichamy M, Arabindoo B, Murugesan V, Enhanced photocatalytic degradation of 4-chlorophenol by Zr^{4+} doped nano TiO_2. Journal of Molecular Catalysis A: Chemical. 2007;266;158-165.
26. Sing KSW, Reporting physisorption data for gas/solid systems with special reference to the determination of surface area and porosity (Recommendations 1984). Pure and applied chemistry. 1985;57;603-619.
27. Mugundan S, Rajamannan B, Viruthagiri G, Shanmugam N, Gobi R, Praveen P, Synthesis and characterization of undoped and cobalt-doped TiO_2 nanoparticles via sol–gel technique, Applied Nanoscience. 2015; 5;449–456.
28. Bae E, Choi W. Highly enhanced photoreductive degradation of perchlorinated compounds on dye-sensitized metal/ TiO_2 under visible light. Environmental Science &Technology. 2003;37(1);147-52.
29. Guo Q, Guo X, Tian Q. Optionally ultra-fast synthesis of CoO/Co3O4 particles using CoCl2 solution via a versatile spray roasting method. Advanced Powder Technology.2010;21(5);529-33.
30. Vijayan P, Mahendiran C, Suresh C, Shanthi K. Photocatalytic activity of iron doped nanocrystalline titania for the oxidative degradation of 2,4,6-trichlorophenol. Catalysis Today. 2009;141(1);220-4.
31. Yang J, Cui S, Qiao Jq, Lian Hz, The photocatalytic dehalogenation of chlorophenols and bromophenols by cobalt doped nano TiO_2. Journal of Molecular Catalysis A: Chemical. 2014;395;42-51.
32. Li CJ, Wang JN, Wang B, Gong JR, Lin Z, A novel magnetically separable TiO_2/$CoFe_2O_4$ nanofiber with high photocatalytic activity under UV–vis light. Materials Research Bulletin. 2012;47;333-337.
33. Sakthivel S, Shankar M, Palanichamy M, Arabindoo B, Bahnemann D, Murugesan V, Enhancement of photocatalytic activity by metal deposition: characterisation and photonic efficiency of Pt, Au and Pd deposited onTiO_2 catalyst. Water research. 2004;38;3001-3008.
34. Chand R, Obuchi E, Katoh K, Luitel HN, Nakano K, Effect of transition metal doping under reducing calcination atmosphere on photocatalytic property of TiO_2 immobilized on SiO_2 beads. Journal of Environmental Sciences. 2013;25;1419-1423.